Knee Surg Sports Traumatol Arthrosc
DOI 10.1007/s00167-016-4310-z

KNEE

The anterior cruciate ligament: a study on its bony and soft tissue anatomy using novel 3D CT technology

Thomas Tampere[1] · Tom Van Hoof[2] · Michiel Cromheecke[1] · Hans Van der Bracht[3] · Jorge Chahla[4] · Peter Verdonk[5,6,7] · Jan Victor[1]

Received: 31 December 2015 / Accepted: 31 August 2016

Abstract
Purpose The purpose of this study is twofold: first, to visualize both the tibial and femoral bony insertion surfaces and second, to describe the anterior cruciate ligament (ACL) geometrically, using novel 3D CT imaging. In addition, new concepts of best-fit cylinder and central axis are introduced and evaluated.
Methods Eight unpaired knees of embalmed cadavers were used in this study. Following the dissection process, the ACL was injected with a contrast medium for CT imaging. The obtained CT images in extension, 45°, 90° and full flexion were segmented and rendered in 3D allowing morphological and morphometric analysis of the ACL. Anatomical footprint centres, femoral and tibial footprint surface area, best-fit ACL-cylinder intersection area, best-fit ACL-cylinder/footprint coverage ratio, best-fit ACL-cylinder central axis projections at the tibial and femoral footprint in the four positions were used to describe the anatomy of the ACL, based on the Bernard, Hertel and Amis grid.
Results Based on these parameters, with the best-fit cylinder representing the bulk of the ACL, a changing fibre-recruitment pattern was seen with a moving position of the central axis from posterior to anterior on the femoral and tibial footprint, going from extension to flexion. Furthermore, the numerical data show an increase in tibial footprint coverage by the best-fit cylinder through the ACL when the knee is progressively flexed, whereas an inverse relationship was seen on the femoral side.
Conclusion This study is the first to describe the detailed anatomy of the human ACL with respect to its course and footprints using a 3D approach. It confirms the large difference and inter-patient variability between the tibial and femoral footprint area with the former being significantly smaller. The best-fit cylinder concept illustrates the recruitment pattern of the native ACL where in extension the postero-lateral fibres are recruited and in flexion rather the antero-medial bundle, which can be valuable information in reconstructive purposes. The best-fit cylinder and central axis concept offers additional insights into the optimal tunnel placement at the tibial and femoral footprint in order to cover the largest portion of the native ACL soft tissue, aiming for optimal ACL reconstruction.

Keywords Anterior cruciate ligament · 3D · Computerized tomography · Anatomy

✉ Thomas Tampere
ttampere@gmail.com

1 Department of Orthopaedic Surgery and Traumatology, Faculty of Medicine, Ghent University, De Pintelaan 185, 9000 Ghent, Belgium

2 Department of Anatomy, Ghent University, Ghent, Belgium

3 Department of Orthopaedic Surgery and Traumatology, Sint Lucas Ghent, Groenebriel 1, 9000 Ghent, Belgium

4 Steadman Philippon Research Institute, 181W Meadow Dr, Vail, CO 81657, USA

5 Department of Orthopaedic Surgery, Monica Hospitals, Harmoniestraat 68, 2018 Antwerp, Belgium

6 Faculty of Medicine, Ghent University, Ghent, Belgium

7 Department of Orthopaedic Surgery, Antwerp University, Ghent, Belgium

Introduction

Over the past fifty years, ACL reconstruction has known a considerable evolution with recent change of interest to anatomical reconstruction in order to obtain a more

Published online: 13 September 2016

physiological function of the reconstructed ACL [3]. To achieve this goal, there has been extensive research to the anatomy, topography and biomechanical function of the native ACL [11, 13, 21, 26, 30, 40].

To date, ACL's bony insertion sites, its soft tissue anatomy and its orientation were extensively studied and described by 2D imaging methods, going from macroscopic images, up to CT and MRI-based visualization [11, 13, 14, 21, 23, 30, 32, 40]. In spite of the large number of anatomical studies however, recent discussions in the literature concerning ACL reconstruction show that extrapolation of anatomical data to patients' 3D anatomy in the operating theatre seems to remain difficult or even unfeasible [9, 17, 22].

The emergence and recent introduction of 3D imaging techniques in orthopaedic research have led to new insights and caused a wave of innovation within the concept of ACL reconstruction. Recent studies have emphasized the importance of anatomical ACL reconstruction with restoration of normal knee kinematics, antero-posterior translation and rotational stability in order to improve clinical outcome and to slow down progression to/of osteoarthritis [19, 28].

Although a tendency towards anatomical ACL reconstruction suggests thorough knowledge and precise visualization of the ACL footprints and soft tissue anatomy, comprehensive 3D data on native anatomy, serving as a base for the pursuit of anatomical reconstruction, remain however scarce to nonexistent.

Similar analysis of the three-dimensional anatomy of the native PCL resulted in better understanding of the bony anatomy and course of the ligament [36]. New concepts of best-fit cylinder and central axis, taking into account the ACL soft tissues and depicting the ideal tunnel position to enclose the bulk of the ACL fibres, were introduced and evaluated with a view to optimize ACL reconstruction.

Aim of this study is to visualize both the 3D anatomy of the tibial and femoral insertions with accurate reconstruction of the soft tissue, as an attempt to formulate new concepts not only focusing on the bony credentials, nowadays used as the guide for ligamentous reconstruction.

Materials and methods

Eight unpaired knees of embalmed cadavers (four male and four female) without traumatic changes to the cartilage, ligaments or menisci were included. The mean age of the cadavers, at the time of death, was 81.5 (range 66–97 years).

Dissection and contrasting

Dissection of the specimens was performed through an anterior and posterior approach to visualize the ACL. For the anterior approach, the knee was positioned in 90° of flexion. After incising the patellar ligament transversely at joint space level, the infrapatellar fat tissue, the capsular tissue and the synovial structures embedding the ACL were subsequently dissected and removed (Fig. 1).

Posterior dissection was performed with the knee in full extension. In the popliteal fossa, the heads of the gastrocnemius muscles, the tendon of the semimembranosus muscle and the deep popliteal neurovascular bundle were excised to the level of the oblique and the arcuate popliteal ligament and the popliteus muscle. The popliteal tendon was transected at its most lateral visible part where it disappears under the edge of the capsule. From this point, the posterior capsule was transversely opened and with visualization of both cruciates. The dissection procedure was performed with preservation of the lateral and medial parts of the capsule to maintain rotational stability in positioning the knee during CT scanning.

Following dissection, the ACL was labelled and contrasted according to an in-house developed protocol, already successfully used in our previous study on the posterior cruciate [36]. Briefly, the ACL was injected with a contrast medium for (CT) imaging, consisting of 80 % barium sulphate, 10 % glycerine and 10 % water. Toluidine blue powder (0.1 g) was added to stain the solution, which

Fig. 1 Dissection specimen of ACL in extension and full flexion, showing the cruciate as a flat, fan-shaped structure

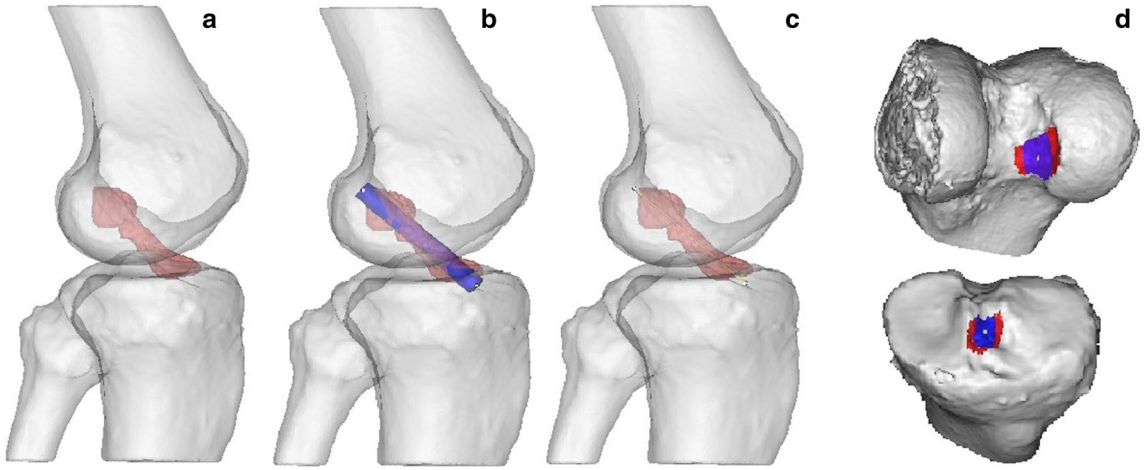

Fig. 2 Three-dimensional representation of ACL, best-fit ACL-cylinder and central axis. **a** 3D reconstruction of ACL (*red*) in semi-transparent knee; **b** ACL (*red*) with best-fit ACL-cylinder (*blue*); **c** ACL (*red*) with central axis (*yellow*); **d** tibial (below) and femoral (above) footprints of ACL (*red*) with intersecting best-fit cylinder (*blue*) and intersecting central axis (*yellow*)

allows a visual control over dispersion and possible leakage of the mixture [6, 20, 37]. A needle (Terumo® needle 0.45 × 23 mm) was inserted between the collagen fibres of the ACL, and the solution was injected with mild pressure until leakage occurred at the injection site or at spots further away along the ligament. Pieces of gauze swabs were wrapped around neighbouring structures and surfaces in order to prevent contamination of possible leaking contrast solution [5].

Then, subsequently, the injection needle was directed towards the femoral and tibial insertion site of the ACL as far as the contact point with the bony surface [8, 29]. On this spot, a small bolus of contrast was injected. Then, a solid injection needle—with identical diameter as the injection needle—was used for repeated picking in this area to obtain maximal absorption of contrast solution in the bony ACL insertion area. This procedure was repeated covering the complete footprint. Additionally, the accessible exterior parts of the ACL were covered with an ethyl acetate-based solution containing lead dioxide to enhance surface contrast [8, 10, 37].

CT scanning

After anatomical preparation, the specimens were visualized by a helical CT scan (Siemens®). Each specimen was scanned in full extension, in 45 and 90 degrees of flexion and in full flexion. The obtained CT images were then imported into Mimics 14.11® software (Materialise N.V., Heverlee, Belgium) allowing to process 2D (CT) images into 3D reconstructions. The resulting 3D rendering of the knee joint and ACL is directly linked to morphological and morphometric analysis tools [37].

Measurements

After the segmentation process, 3D reconstructions were calculated from the selected masks of the native ACL, the distal part of the femoral shaft with the condyles and the tibial plateau in full extension, 45°, 90° and full flexion (Fig. 2a).

For each ACL, cylinders were constructed throughout the entire ligament (including the tibial and femoral footprint). Next the 3D ACL's were virtually sectioned at their midlevel in the transverse plane (Fig. 3). Based on these midsections of the ligament, best-fit ACL-cylinders were calculated and oriented along the native orientation of the bulk of the ligament. This was done for each ACL in each of the reconstructed degrees of flexion (Fig. 2b).

Femoral and tibial footprint surface area, geometric centre of the footprints, best-fit ACL-cylinders, best-fit ACL-cylinder intersection area, best-fit ACL-cylinder/footprint coverage ratio and best-fit ACL-cylinder central axis projections at the tibial and femoral footprint were used to describe the anatomy of the ACL. All surface areas were calculated using 3-matic® software (Materialise N.V., Heverlee Belgium) (Fig. 2c, d) [35].

The anatomical centres of the footprints and central axis intersections were projected on the footprint and localized on the tibial and femoral insertion sites using grids according to the quadrant method of Amis, Bernard and Hertel [1, 2] (Fig. 4a, b). On the femoral side, grids were constructed, using AutoCAD® 2012 (San Rafael, CA) for each knee in full extension, 45°, 90° and full flexion, on a strict profile view of the 3D reconstructed knee. Subsequently, a 4 × 4 grid was drawn, aligned according to the most anterior line of the femoral notch, from the anterior to posterior edge of

the femur. The other lines were constructed perpendicular to the posterior line, tangent to the condyle. The tibial grid was constructed starting from a line parallel to the posterior and anterior wall of the tibial plateau, with the medial and lateral border perpendicular to the posterior reference. Based on these grids, coordinates were assigned to the anatomical centre of the footprint and to the central axis in cranio-caudal and posterior–anterior direction for the femur on the one hand, and in medio-lateral and antero-posterior direction for the tibia [34, 35].

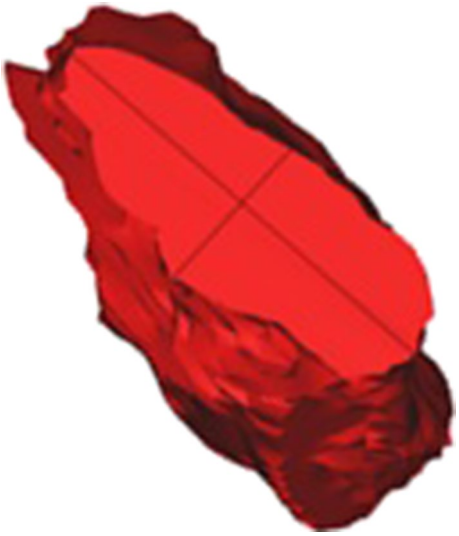

Fig. 3 Virtual section at the midportion of the ACL in the transverse plane

Data analysis

Mean (SD) surface areas ($mm^2 \pm 1$ SD) were calculated for the tibial and femoral native ACL insertion site. Then, the mean intersection areas ($mm^2 \pm 1$ SD) of the best-fitted ACL-cylinder with the tibial and femoral footprint surfaces were calculated and expressed as a mean coverage (% ± 1 SD) in relation to the complete footprint areas. The areas of the femoral and tibial footprints and native ACL diameter were compared to the femoral epicondylar mediolateral width, using a Spearman's rank correlation coefficient. This statistical test was also used to evaluate correlations between the tibial and femoral coverage ratios. To determine differences between the femoral and tibial footprint area and between the femoral and tibial intersection areas, a Mann–Whitney *U* test was used. The level of significance was set at $p < 0.05$.

Results

ACL footprints

The mean footprint surface area of the tibial and femoral footprint was 159.2 mm^2 (SD ± 31.3) and 194.5 mm^2 (SD ± 38.3), respectively, with a tibia/femur ratio of 0.84. The mean femoral epicondylar width was 83.9 mm (SD ± 3.8). A high inter-patient variability was observed, with Spearman's Rho correlation coefficient 0.26 (p = n.s.), showing no significant correlations between the femoral and the tibial footprint areas. Comparing the

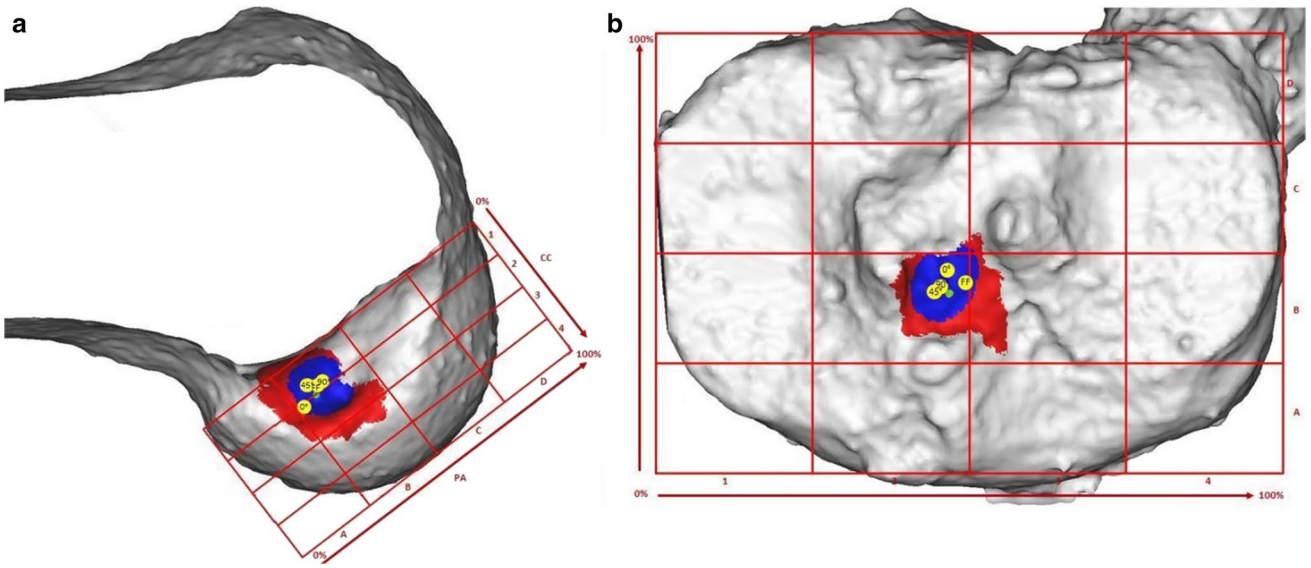

Fig. 4 Three-dimensional representation of the femoral (**a**) and tibial (**b**) ACL footprint (*red*) with intersection of the best-fit ACL-cylinder (*blue*), the central axis (*yellow*) in full extension, 45°, 90° of flexion and in full flexion. The anatomical centre is represented in *green*. The overlying grids were used to determine coordinates of each intersection

Table 1 Surfaces of intersections between the best-fit ACL-cylinders and the tibial/femoral footprint, with coverage ratios, in 0°, 45°, 90° and in full flexion

	0°	45°	90°	Full flexion
Best-fit cylinder –tibial footprint intersection	55.1 mm^2 (SD ± 13.1)	79.7 mm^2 (SD ± 19.8)	93.0 mm^2 (SD ± 29.1)	108.3 mm^2 (SD ± 48.0)
Coverage ratio	35.4 % (SD ± 9.3)	50.7 % (SD ± 12.3)	57.8 % (SD ± 12.5)	63.3 % (SD ± 17.5)
Best-fit cylinder –femoral footprint intersection	110.3 mm^2 (SD ± 17.8)	104.8 mm^2 (SD ± 31.3)	77.6 mm^2 (SD ± 22.7)	75.5 mm^2 (SD ± 28.7)
Coverage ratio	58.4 % (SD ± 12.6)	53.5 % (SD ± 11.8)	40.8 % (SD ± 12.5)	38.9 % (SD ± 11.4)

tibial (Spearman 0.3, p = n.s.) and femoral (Spearman 0.07, p = n.s.) footprint areas to the femoral epicondylar width, no significant correlations were found.

ACL best-fit cylinders

Mean diameters of the best-fit cylinder through the midsection of each ACL in 0°, 45°, 90° of flexion and in full flexion were 7.7 mm (SD ± 0.8), 7.9 mm (SD ± 0.9), 7.9 mm (SD ± 0.8) and 8.5 mm (SD ± 0.9), respectively. These data show an increase of diameter of the best-fit cylinder during range of motion.

Then, again for each knee in the various degrees of flexion, the surface area was calculated of the intersection between the best-fit cylinder (cylinder fitting the entire cruciate ligament with diameter adjustment to the midsection cylinder), and the tibial and femoral footprint of the ACL. On the tibial side, the mean intersection surface was 55.1 mm^2 (SD ± 13.2) at 0°, 79.7 mm^2 (SD ± 19.8) at 45°, 93.0 mm^2 (SD ± 29.1) at 90° and 108.3 mm^2 (SD ± 48.0) in full flexion.

Mean femoral intersection surfaces were 110.3 mm^2 (SD ± 17.9) in extension, 104.8 mm^2 (SD ± 31.3) at 45°, 77.6 mm^2 (SD ± 22.7) at 90° and 75.5 mm^2 (SD ± 28.7) in full flexion (Table 1).

These data point out that, during transition from full extension to full flexion, the tibial intersection of the best-fit cylinder becomes larger, with a decreasing femoral intersection.

Same results were seen for the percentage of tibial footprint coverage at 0° of flexion a coverage of 35.4 % (SD ± 9.3), at an angle of 45° 50.7 % (SD ± 27.1) at 90° 57.9 % (SD ± 12.5) and at full flexion 63.3 % (SD ± 17.5). Average femoral coverage was 58.4 % (SD ± 12.6), 53.7 % (SD ± 11.8), 40.8 (SD ± 12.5) and 38.9 % (SD ± 11.4), respectively. From these data, it was again inferred that the tibial coverage increases, while femoral coverage decreases with increasing flexion.

At full extension, no significant correlation could be withheld between the best-fit cylinder coverage of the tibial and femoral footprint (Spearman's rank correlation coefficient of −0.14, p = n.s.) nor at full flexion (Spearman 0.64, p = n.s.). On the other hand however, a significant positive correlation was seen with respect to the tibial and femoral coverage at 45° (Spearman 0.88, p = 0.004) and 90° of flexion (0.71 Spearman, p = 0.047) (Table 1).

3D anatomical centre of the footprint

The 3D anatomical centre of the tibial and femoral footprint was calculated and visualized on each insertion site; based on the aforementioned quadrant methods, coordinates were assigned to these centres with an average position at 49.3 % (SD ± 2.1) compared to the medio-lateral distance of the tibial plateau and 39.7 % (SD ± 2.9), plotted against the anterior–posterior axis.

On the femoral side, the mean position of the femoral footprint centre was situated at 32.6 % (SD ± 3.8) along the posterior–anterior axis and at 19.9 % (SD ± 5.9) in cranio-caudal direction.

Central axis of the ACL

For each knee, the central axis of the best-fit cylinder was determined for every studied degree of flexion and located using the quadrant method. At the tibial footprint, in full extension, the average ACL-centre was located at 48.8 % (SD ± 1.7) along the medio-lateral axis and at 43.1 % (SD ± 5.2) in antero-posterior direction. In 45° flexion, we obtained a medio-lateral position of 48.3 % (SD ± 2.5) and anterior–posterior 40.1 % (SD ± 3.8). At 90° flexion, coordinates were 48.1 % (SD ± 1.9) and 39.7 % (SD ± 4.5) in medio-lateral and antero-posterior direction, respectively. At full flexion, an average mid-lateral localization of 48.4 % (SD ± 2.6) and anterior–posterior at 38.0 % (SD ± 6.7) was seen. In full flexion, no intersection could be constructed in two out of eight knees, between the central axis and the tibial footprint because of lack of intersection between both surfaces.

At the femoral footprint, in full extension, average position was projected at 22.9 % (SD ± 3.6) postero-anteriorly and in cranio-caudal direction at 21.5 % (SD ± 2.5). In 45° flexion at 28.3 % (SD ± 5.3) and at 10.3 % (SD ± 6.6), respectively. At 90° of flexion, coordinates of the central

axis were 33.3 % (SD ± 3.5) and 14.7 % (SD ± 9.3) in postero-anterior and cranio-caudal direction. When giving full flexion, the central axis was located at 34.9 % (SD ± 4.4) and cranio-caudally at 13.4 % (SD ± 5.3). There was no intersection between the central axis and the femoral footprint in four out of eight knees in full extension and in two of them, at 45° of flexion. These data, with the best-fit cylinder representing the bulk of the ACL, show a changing fibre-recruitment pattern with a moving position of the central axis from posterior to anterior on the femoral and tibial footprint, going from extension to flexion (Fig. 5) (Table 2).

Discussion

This study describes, as one of the first, the detailed 3D anatomy of the human ACL with respect to its course and footprints using a direct contrast-enhanced visualization methodology based on CT imaging. As yet proven in previous work on the posterior cruciate [36], this unique approach offers valuable information on the bony insertion sites, but also formulates new insights into optimal tunnel placement based on the new conduct of best-fit cylinder and central axis; a reasoning on soft tissue visualization that allows maximum ligamentous soft tissue coverage to the mid-footprint anatomical approach which only allows maximum bony footprint coverage. The best-fit cylinder concept was chosen because it more or less equals today frequently used cylindrical grafts (hamstring autografts) in ACL reconstruction, and it allows better understanding of graft behaviour and offers an automated tool for native soft tissue modelling.

This study shows a significantly smaller tibial ACL insertion when compared to the femoral insertion. The large discrepancy between the two surfaces, as found in our study, with important inter-patient variability of the footprint sizes, is confirmed by similar findings in the reports of Siebold et al. [24, 25]. Comparing both surfaces, a tibia/femur ratio of 84 % was seen. This finding is in contrast with data from the literature, describing an inverse relationship going from 120 to 154 % [4, 7, 12, 16, 18, 24, 25]. Possible explanations for this discrepancy are the relatively small number of subjects studied and the relatively high age of cadavers with suspicion of osteophyte overgrowth. Secondly, all measurements were taken on 3D reconstructions, whereas 2D analysis was used in previous papers on the subject. Extrapolation of our data to 2D reconstruction, however, showed a ratio of 87 %.

Concentrating on the bulk of the ACL, a fanning out was seen towards the tibial and femoral footprint. During range of motion to full flexion, whether or not taking into account the footprints, a significant increase of the best-fit

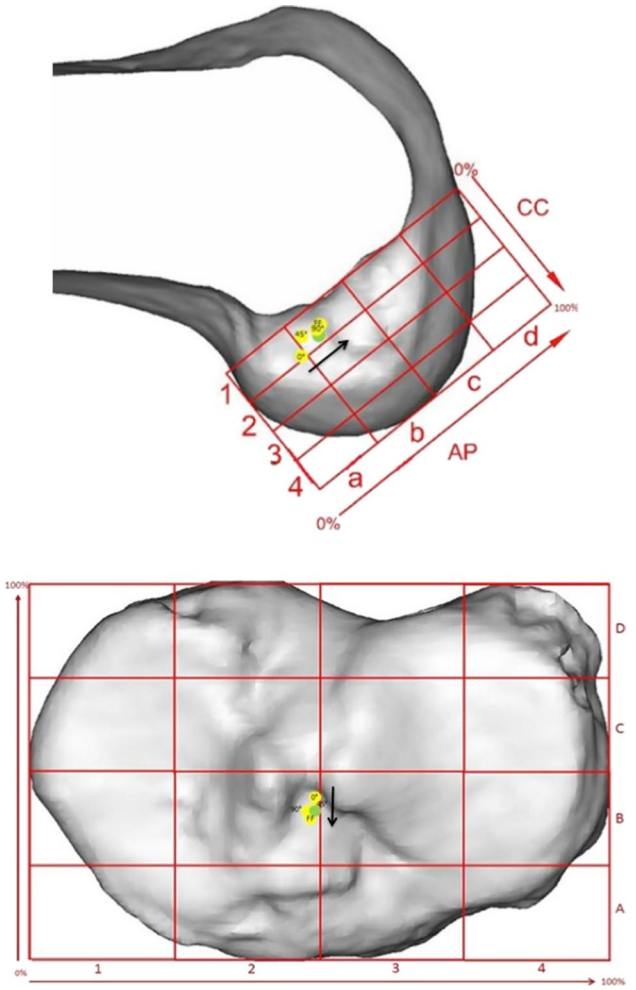

Fig. 5 Three-dimensional representation of the mean position of the femoral and tibial anatomical centre (*green*) and the mean position of the central axis in extension, 45°, 90° and in full flexion. The overlying grids were used to determine coordinates of each intersection. The *black arrow* indicates movement of the central axis during range of motion

cylinder diameter was seen, causing a stretched oval shape of the ACL-transection in deep flexion. This finding may be of importance in determining the diameter of the graft of ACL reconstruction. Furthermore, with an increase in the degree of flexion, an increase of tibial footprint coverage was seen, with a maximum covering in full flexion of 63 %. With regard to the femoral footprint, a decrease in coverage was seen during increasing degree of flexion with a maximum coverage of the soft tissue cylinder of 58 % in full extension. This observation may be of importance in the context of reconstructive purposes, and occurrence of 'killer angles', as drilling angles can influence the percentage of soft tissue coverage of the native footprints [34, 35].

Data on exact position of the AM and PL bundles of the ACL are scarce. A comparison with data from the literature about these coordinates is not easy since data

Table 2 Coordinates of the anatomical centre of the femoral and tibial footprint in combination with the coordinates of the central axis intersections with the ACL footprint during range of motion

	Anatomical centre (%)	0° (%)	45° (%)	90° (%)	Full flexion (%)
Tibial footprint					
Medio-lateral	49.3	48.8	48.1	48.1	48.4
Antero-posterior	39.7	43.1	40.2	39.7	38.0
Femoral footprint					
Postero-anterior	32.6	22.9	28.3	33.3	34.9
Cranio-caudal	19.9	21.5	10.3	14.7	13.4

were obtained using different visualization and measurement methods, because of which, to date, there is no consensus about the exact location of the anatomical centre of the footprint. On the femoral side, Tsukada et al. [33] described a femoral AM position of 17.8 % (±2.9) cranio-caudally and 25.9 % (±2.0) in postero-anterior direction. The PL bundle was located at 42.1 % (±3.9) and 34.8 % (±5.0), respectively. Yamamoto et al. [38] found the AM bundle in cranio-caudal direction at 16 % (±5.0) and 25 % (±5.0) postero-anteriorly. 42 % (±3.0) and 29 % (±6.0) were the coordinates of the PL bundle. Takahashi et al. [30, 31] found in their dissections the AM bundle in cranio-caudal direction at 26.9 and 31.9 %. The PL bundle was seen at 53.2 and 39.8 %, respectively. Bernard et al. [2] and Musahl et al. [13] did not separate the AM and PL bundle but calculated position of the ACL at 28.5 and 26 % in cranio-caudal direction and in postero-anterior direction at 24.8 and 27 %. These data are close to our findings concerning the position of the anatomical centre of the footprint, showing a 3D position of the ACL-centre close to the position of the AM bundle in cranio-caudal direction. Antero-posteriorly, the 3D anatomical centre seems to appear close to the PL bundle.

Comparing antero-posterior positions of the central axis of the best-fit cylinder during range of motion to data from the literature, a trend was seen with in full extension a position of the central axis close to the PL bundle and with progressive flexion moving to a position close to the AM bundle insertion. In cranio-caudal direction however, the central axis of the best-fit cylinder stays close to the AM position.

Concerning the tibial insertion, data are even more limited. Yamamoto et al. [38] described a tibial AM bundle at 37.6 % AP and 46.5 % in medio-lateral direction. The PL bundle was located at 50.1 and 51.2 %, respectively. Bernard et al. [2] described only an antero-posterior direction of the ACL at 44 %. Staubli et al. [27] described an antero-posterior location of the AM and PL bundle at 28.6 and 32.1 %, respectively. Compared to our 3D data, our anatomical tibial ACL-centre and the central axis of the best-fit cylinder can be located between the AM and PL bundle, but however moving from posterior to anterior during range of motion from extension to full flexion, proving a changing recruitment pattern of ACL fibres (Figs. 1, 5).

Based on these data, early and prudent assumptions of the existence of an ACL functional axis/functional centre can be made, with a changing femoral and tibial position of the central axis during range of motion.

Comparing the best-fit cylinder central axis to the determined geometric centre of the footprint an overlap in only 25 % was seen with a changing position of the femoral intersection of the best-fit cylinder central axis during increase in degree of flexion. This was seen in one case in 45° of flexion, in two cases during full flexion and in one subject in 90° of flexion. A tibial overlap was also seen in only 25 %, between the anatomical centre and the central axis of the best-fit cylinder; three central axes covered the anatomical centre in extended position and in one case in 45° of flexion. Based on these findings, early assumptions of the existence of a functional ACL-centre, 'wandering' around the anatomical centre during range of motion, can be made. One should therefore, during tunnel positioning in ACL reconstruction, keep in mind that there might exist a functional ACL-centre, differing from the anatomical centre. In terms of reconstruction, there is not yet consensus regarding the superiority of single-bundle versus double-bundle ACL reconstruction. Furthermore, discussions about optimal tunnel placement during single-bundle reconstruction are still going on whether one should use an AM–AM, AM–PL or a PL–PL configuration to obtain translational and rotational stability [15]. In this regard, a best-fit cylinder approach may offer a more balanced ACL reconstruction, because it does not rely on the mid-position of the footprints, but rather on the bulk of soft tissues of the ACL, taking into account the relative size of the AM bundle as well as of the PL bundle.

However, several limitations of the present study should be addressed. First, a relatively limited number of subjects were studied. Second, the age of the human cadavers did not represent the average, typical age for population that sustains ACL injury. Third, the antero-medial (AM) and postero-lateral (PL) bundle of the ACL, as described in 2D anatomical studies [16, 30, 39] could not be isolated on the 3D reconstructions.

Conclusion

With three-dimensional visualization of the ACL footprints and its soft tissue anatomy, this study is one of the first to describe the detailed anatomy of the human ACL with respect to its course and footprints using a unique 3D approach. A significant inter-patient variability in footprint size was seen with remarkable discrepancy between femoral and tibial footprint surfaces. Using the best-fit cylinder and central axis concept, an accurate evaluation could be made of the anatomical centre and the central axis position of the ACL footprint during the whole range of motion, suggesting a functional centre of the anterior cruciate. The best-fit cylinder concept illustrates the recruitment pattern of the native ACL fibres where in extension the posterolateral fibres are recruited and in flexion rather the anteromedial bundle, which can be valuable information in reconstructive purposes. This concept offers additional insights and may lead to improvement of ACL reconstruction.

Compliance with ethical standards

Conflict of interest The authors declare that they have no conflict of interest.

Funding No funding was received for this study.

Ethical approval In these testaments is stated that the human body can be implemented in educational or research programs with no further specification. The body donation program guarantees high ethical standards during implementation of the human body in the different projects.

Informed consent In the Ghent Anatomical Facility informed consent for anatomical study is given as people voluntary sign up for the body donation program.

References

1. Amis A, Jakob R (1998) Anterior cruciate ligament graft positioning, tensioning and twisting. Knee Surg Sports Traumatol Arthrosc 6:S2–S12
2. Bernard M, Hertel P, Hornung H, Cierpinski T (1997) Femoral insertion of the ACL. Radiographic quadrant method. Am J Knee Surg 10:14–22
3. Chambat P, Guier C, Sonnery-Cottet B, Fayard J-M, Thaunat M (2013) The evolution of ACL reconstruction over the last fifty years. Int Orthop 37:181–186
4. Dargel J, Pohl P, Tzikaras P et al (2006) Morphometric side-to-side differences in human cruciate ligament insertions. Surg Radiol Anat 28:398–402
5. De Maeseneer M, Jager T, Vanderdood K, Van Roy P, Shahabpour M, Marcelis S (2003) Ultrasound during dissection of cadaveric specimens: a new method for obtaining ultrasound-anatomic correlations in musculoskeletal radiology. Eur Radiol 14:870–874
6. Feigl G, Fuchs A, Gries M, Hogan QH, Weninger B, Rosmarin W (2006) A supraomohyoidal plexus block designed to avoid complications. Surg Radiol Anat 28:403–408
7. Ferretti M, Ekdahl W, Shen W et al (2007) Osseous landmarks of the femoral attachment of the anterior cruciate ligament: an anatomic study. Arthroscopy 23:1218–1225
8. Forsythe B, Harner C, Martins CA, Shen W, Lopes OV Jr, Fu FH (2009) Topography of the femoral attachment of the posterior cruciate ligament. Surgical technique. J Bone Joint Surg Am 91(1):89–100
9. Frobell R, Roos H, Roos E, Roemer F, Ranstam J, Lohmander S (2013) Treatment for acute anterior cruciate ligament tear: five year outcome of randomized trial. BMJ 346:f232. doi:10.1136/bmj.f232
10. Groscurth P, Eggli P, Kapfhammer J, Rager G, Hornung JP, Fasel JDH (2001) Gross anatomy in the surgical curriculum in Switzerland: improved cadaver preservation, anatomical models, and course development. Anat Rec (New Anat) 265:254–256
11. Hara K, Mochizuki T, Sekiya I, Yamaguchi K, Akita K, Muneta T (2009) Anatomy of normal human anterior cruciate ligament attachments evaluated by divided small bundles. Am J Sports Med 37:2386–2391
12. Harner CD, Baek GH, Vogrin TM, Carlin GJ, Kashiwaguchi S, Woo SL (1999) Quantitative analysis of human cruciate ligament insertions. Arthroscopy 15:741–749
13. Hwang M, Piefer J, Lubowitz J (2012) Anterior cruciate ligament tibial footprint anatomy: systematic review of the 21st century literature. Arthroscopy 28:728–734
14. Inderdaug E, Larsen A, Strand T et al (2016) The effect of feedback from post-operative 3D CT on placement of femoral tunnels in single-bundle anatomic ACL reconstruction. Knee Surg Sports Traumatol Arthrosc 24(1):154–160
15. Kato Y, Maeyama A, Lertwanich P, Wang J, Ingham S, Kramer S, Martins C, Smolinski P, Fu F (2014) Biomechanical comparison of different graft positions for single-bundle anterior cruciate ligament reconstruction. Knee Surg Sports Traumatol Arthrosc 21:816–823
16. Luites JW, Wymenga AB, Blankevoort L et al (2007) Description of the attachment geometry of the anteromedial and posterolateral bundles of the ACL from arthroscopic perspective for anatomical tunnel placement. Knee Surg Sports Traumatol Arthrosc 15:1422–1431
17. McCullough K, Phelps K, Spindler K, Matava M, Dunn W, Parker R, Reinke E (2012) Return to high school- and college-level football after anterior cruciate ligament reconstruction. Am J Sports Med 40:2523–2529
18. Muneta T, Takakuda K, Yamamoto H (1997) Intercondylar notch width and its relation to the configuration and cross-sectional area of the anterior cruciate ligament. A cadaveric knee study. Am J Sports Med 25:69–72
19. Norris R, Thompson P, Getgood A (2012) The effect of anterior cruciate ligament reconstruction on the progression of osteoarthritis. Open orthop J 6:506–510
20. Pfirrmann CW, Oberholzer PA, Zanetti M, Boos N, Trudell DJ, Resnick D, Hodler J (2001) Selective nerve root blocks for the treatment of sciatica: evaluation of injection site and effectiveness. A study with patients and cadavers. Radiology 221:704–711
21. Piefer J, Pflugner R, Hwang M, Lubowitz J (2012) Anterior cruciate ligament femoral footprint anatomy: systematic review of the 21st century literature. Arthroscopy 28:872–881
22. Rahr-Wagner L, Thillemann T, Pedersen A, Lind M (2013) Increased risk of revision after anteromedial compared with transtibial drilling of the femoral tunnel during primary anterior cruciate ligament reconstruction: results from the Danish knee ligament Reconstruction register. Arthroscopy 29:98–105
23. Robbrecht C, Claes S, Cromheecke M et al (2014) Reliability of a semi-automated 3D-CT measuring method for tunnel

diameters after anterior cruciate ligament reconstruction: a comparison between soft-tissue single-bundle allograft vs. autograft. Knee 21(5):926–931
24. Siebold R, Ellert T, Metz S et al (2008) Femoral insertions of the anteromedial and posterolateral bundles of the anterior cruciate ligament: morphometry and arthroscopic orientation models for double-bundle bone tunnel placement—a cadaveric study. Arthroscopy 24:585–592
25. Siebold R, Ellert T, Metz S et al (2008) Tibial insertions of the anteromedial and posterolateral bundles of the anterior cruciate ligament: morphometry, arthroscopic landmarks, and orientation model for bone tunnel placement. Arthroscopy 24:145–161
26. Smigielski R, Zdanowicz U, Drwiega M et al (2015) Ribbon like appearance of the midsubstance fibres of the anterior cruciate ligament close to its femoral insertion site: a cadaveric study including 111 knees. Knee Surg Sports Traumatol Arthrosc 23(11):3143–3150
27. Staubli H, Rauschning W (1994) Tibial attachment area of the anterior cruciate ligament in the extended knee position. Anatomy and cryosections in vitro complemented by magnetic resonance arthrography in vivo. Knee Surg Sports Traumatol Arthrosc 2:138–146
28. Struewer J, Ziring E, Frangen TM, Efe T, Meißner S, Buecking B, Bliemel C, Bernd Ishaque (2013) Clinical outcome and prevalence of osteoarthritis after isolated anterior cruciate ligament reconstruction using hamstring graft: follow-up after two and ten years. Int Orthop 37:271–277
29. Tajima G, Nozaki M, Iriuchishima T, Ingham SJ, Shen W, Smolinski P, Fu FH (2009) Morphology of the tibial insertion of the posterior cruciate ligament. J Bone Joint Surg Am 91(4):859–866
30. Takahashi M, Doi M, Abe M, Suzuki D, Nagano A (2006) Anatomical study of the femoral and tibial insertions of the anteromedial and posterolateral bundles of human anterior cruciate ligament. Am J Sports Med 34:787–792
31. Takahashi M, Matsubara T, Doi M, Suzuki D, Nagano A (2006) Anatomical study of the femoral and tibial insertions of the anterolateral and posteromedial bundles of human posterior cruciate ligament. Knee Surg Sports Traumatol Arthrosc 14:1055–1059
32. Taketomi S, Inui H, Nakamura K et al (2014) Clinical outcome of anatomic double-bundle ACL reconstruction and 3D CT model-based validation of femoral socket aperture position. Knee Surg Sports Traumatol Arthrosc 22(9):2194–21201
33. Tsukada H, Ishibashi Y, Tsuda E, Fukuda A, Toh S (2008) Anatomical analysis of the anterior cruciate ligament femoral and tibial footprints. J Orthop Sci 13:122–129
34. Van der Bracht H, Bellemans J, Victor J, Page B, Verdonk P (2014) Can a tibial tunnel in ACL surgery be placed anatomically without impinging on the femoral notch? A risk factor analysis. Knee Surg Sports Traumatol Arthrosc 22(2):291–297
35. Van der Bracht H, Verhelst L, Stuyts B, Page B, Bellemans J, Verdonk P (2014) Anatomic single-bundle ACL surgery: consequences of tibial tunnel diameter and drill-guide angle on tibial footprint coverage. Knee Surg Sports Traumatol Arthrosc 22(5):1030–1039
36. Van Hoof T, Cromheecke M, Tampere T, D'herde K, Victor J, Verdonk P (2013) The posterior cruciate ligament: a study on its bony and soft tissue anatomy using novel 3D CT technology. Knee Surg Sports Traumatol Arthrosc 21:1005–1010
37. Van Hoof T, Gomes GT, Audenaert E, Verstraete K, Kerckaert I, D'Herde K (2008) 3D computerized model for measuring strain and displacement of the brachial plexus following placement of reverse shoulder prosthesis. Anat Rec (Hoboken) 291:1173–1185
38. Yamamoto Y, Hsu WH, Woo SL, Van Scyoc AH, Takakura Y, Debski RE (2004) Knee stability and graft function after anterior cruciate ligament reconstruction: a comparison of a lateral and anatomical femoral tunnel placement. Am J Sports Med 32:1825–1832
39. Zantop T, Herbort M, Raschke MJ et al (2007) The role of the anteromedial and posterolateral bundles of the anterior cruciate ligament in anterior tibial translation and internal rotation. Am J Sports Med 35:223–227
40. Zantop T, Petersen W, Sekiya J, Musahl V, Fu F (2006) Anterior cruciate ligament anatomy and function relating to anatomical reconstruction. Knee Surg Sports Traumatol Arthrosc 14:982–992